Graphical representation of constitutive equations

Gerd Gudehus, o. Prof. em. Dr.-Ing. Dr. h.c.

Professor Emeritus
University of Karlsruhe
Institute of Soil Mechanics and Rock Mechanics
Engler-Bunte-Ring 14
76131 Karlsruhe, Germany
E-mail: Gerd.Gudehus@ibf.uni-karlsruhe.de
Tel: +49 721 6082220, Fax: +49 721 696096

David Mašín[1], RNDr., M. Phil., Ph. D.

Senior Lecturer
Charles University in Prague
Faculty of Science
Institute of Hydrogeology, Engineering Geology and Applied Geophysics
Albertov 6
12843 Prague 2, Czech Republic
E-mail: masin@natur.cuni.cz
Tel: +420-2-2195 1552, Fax: +420-2-2195 1556

July 9, 2008

Number of words: 1975 plus References and figure captions
Number of tables: 0
Number of figures: 7

Accepted version of a Technical Note for *Géotechnique*

[1]Corresponding author

Keywords

Constitutive relations, elasticity, plasticity, shear strength, stiffness

Introduction

Many theories, based on different mathematical approaches, emerged from the research on soil constitutive modelling. Even though the models may be developed to be easy to use, with low number of parameters and well-defined calibration procedures, their mathematical formulations are often rather complex and only few scientists, working on their development, understand it into detail. In this Note we propose a way for *graphical* (as opposed to algebraic) representation of the most important soil properties captured by the models, which eases judgment of their response capabilities and reveals their physical grounds without need for understanding details of their mathematical formulations.

We focus on a polar representation of tangential stiffness for different strain rate directions and on representation of *state limits*, defined as states attained asymptotically by *proportional* deformation paths (i.e., deformation paths with constant strain rate directions). Constitutive relations of rate type

$$\dot{\boldsymbol{\sigma}}' = f(\boldsymbol{\sigma}', e, \dot{\boldsymbol{\epsilon}}) \tag{1}$$

are studied, with $\boldsymbol{\sigma}'$ being effective Cauchy stress, e void ratio and $\dot{\boldsymbol{\epsilon}}$ the strain rate. In this Note we restrict our attention to cylindrical symmetry. Moreover, rate-independence is presumed, i.e. the function f satisfies

$$f(\boldsymbol{\sigma}', e, \lambda\dot{\boldsymbol{\epsilon}}) = \lambda f(\boldsymbol{\sigma}', e, \dot{\boldsymbol{\epsilon}}) \tag{2}$$

for any $\lambda > 0$. We consider purely frictional material which cannot attain tensile stresses.

For cylindrical symmetry the stress state may be fully characterised by the effective stress components σ'_1 and $\sigma'_2 = \sigma'_3$, and the strain rate by components $\dot{\epsilon}_1$ and $\dot{\epsilon}_2 = \dot{\epsilon}_3$. To represent stress obliquity and strain rate direction, we define an angle ψ_σ in the plane σ'_1 vs. $\sqrt{2}\sigma'_2$ (Fig. 1a), and angle $\psi_{\dot{\epsilon}}$ in the plane $\dot{\epsilon}_1$ vs. $\sqrt{2}\dot{\epsilon}_2$ (Fig. 1b).

The following special directions of ψ_σ and $\psi_{\dot{\epsilon}}$ will be distinguished: Direction i which corresponds to isotropic loading ($\sigma'_1 = \sigma'_2$ and $\dot{\epsilon}_1 = \dot{\epsilon}_2$) with $\psi_\sigma(i) = 0°$ and $\psi_{\dot{\epsilon}}(i) = 0°$, directions $\pm c$ which correspond to critical state conditions in compression and extension with $\psi_{\dot{\epsilon}}(c) = 90°$, $\psi_{\dot{\epsilon}}(-c) = -90°$ and $\psi_\sigma(\pm c)$ related to the critical state friction angle φ_c through

$$\psi_\sigma(\pm c) = \pm\tan^{-1}\left(\frac{2\sqrt{2}\sin\varphi_c}{3 \mp \sin\varphi_c}\right) \tag{3}$$

and unattainable limit bounds $\pm d$ which correspond to *axial splitting* with $\sigma'_2 = 0$ and $\dot{\epsilon}_1 = 0$ and *discing* with $\sigma'_1 = 0$ and $\dot{\epsilon}_2 = 0$, i.e. $\psi_{\dot{\epsilon}}(d) \simeq 144.7°$, $\psi_{\dot{\epsilon}}(-d) \simeq -125.3°$, $\psi_\sigma(d) \simeq 54.7°$ and $\psi_\sigma(-d) \simeq -35.3°$.

Graphical representation of tangential stiffness

Gudehus (1979) proposed so-called *response envelopes* as a powerful tool for representing constitutive equations of rate type. The response envelopes are polar diagrams for unit strain rates, i.e. for

$$D = \sqrt{\dot{\epsilon}_1^2 + 2\dot{\epsilon}_2^2} = 1 \tag{4}$$

as plotted in the plane $\dot{\sigma'}_1$ vs. $\sqrt{2}\dot{\sigma'}_2$ (Fig. 2). Response envelopes visualise the tangential stiffness predicted by a model for different $\dot{\boldsymbol{\epsilon}}$ directions (the larger the distance from the

origin, the higher the stiffness), their shape and size depend on the constitutive model and on the state variables $\boldsymbol{\sigma}'$ and e. To enhance the informative value of the polars, labels and graphical symbols are added for particular directions of $\dot{\boldsymbol{\epsilon}}$ as defined in the Introduction. Response envelopes are often mapped from the stress rate space into the stress space, which reveals the influence of the stress state on the tangential stiffness.

Response envelopes for the Modified Cam clay model by Roscoe and Burland (1968)[1] are plotted in Fig. 3 in order to demonstrate the representation. The stress states correspond to different positions with respect to the elliptic yield surface of the model, which is also indicated in the figure. Response envelopes for states inside the yield surface (*oc1* and *oc2*), corresponding to a hypoelastic response, are elliptic and centred about the reference stress state. The elastic shear and bulk moduli G and K are revealed by the size of the envelopes, their ratio is represented by the slenderness of the envelopes. The envelope for state *oc1* (100 kPa) is twice as big as envelope for state *oc2* (50 kPa), but their aspect ratios are the same, showing that both G and K are proportional to the mean stress and their ratio is constant. The response envelope for an isotropic normally consolidated state (i) is composed of two elliptic sections. Both are centred about the reference stress, one corresponds to elastic unloading, the second to elasto-plastic loading. The response envelope is continuous thanks to the elasto-plastic consistency condition. The loading section has another aspect ratio than the unloading section, showing a smaller bulk modulus for isotropic loading than for unloading. The envelopes for critical states in compression (c) and extension ($\text{-}c$) are also composed of two elliptic sections. The section representing elasto-plastic loading is now reduced to a straight line, revealing that the model predicts zero stress rate for elasto-plastic loading at a critical state.

Graphical representation of state limits

State limits are defined as states approached asymptotically by monotonous deformations with constant $\psi_{\dot{\epsilon}}$. They may be denoted as *attractors* of soil behaviour as they can be attained irrespective of the initial state. Similar asymptotic properties were introduced as swept-out-memory (SOM) by Gudehus et al. (1977), more details can be found in Gudehus (2008). State limits represent fundamental characteristics of soil behaviour which should be captured by constitutive models. They can be represented by plots as shown in Fig. 4. In the p' vs e plane, physically admissible states are bound by the limit void ratios e_i and e_d. The limit void ratios decrease affinitively with increasing p' (Fig. 4a). A *relative void ratio* r_e may be defined as

$$r_e = \frac{e - e_d}{e_c - e_d} \tag{5}$$

with e_c and e_d corresponding to the current mean stress p' according to Fig. 4a. For state limits r_e depends on ψ_σ as shown in Fig. 4b, and $\psi_{\dot{\epsilon}}$ depends on ψ_σ as plotted in Fig. 4c.

For an *isotropic* compression (i) the void ratio e_i for a given p' is the highest possible one, r_e is maximal and ψ_σ and $\psi_{\dot{\epsilon}}$ are equal to 0° from their deffinitions. For proportional stretching along *contractant* paths the stress and strain rate angles ψ_σ and $\psi_{\dot{\epsilon}}$ are in the sectors between c and $-c$, and r_e exceeds 1. The critical void ratio e_c that corresponds to stretching with constant volume ($\psi_{\dot{\epsilon}}(\pm c)$) is in between e_i and e_d. The two ψ_σ for *critical states* (labelled c and $-c$) are given by Eqn. (3), related $\psi_{\dot{\epsilon}}$ were also given above. The same e is presumed for c and $-c$ and a given p', thus $r_e = 1$ holds by Eqn. (5). For *dilatant* paths the stress state is outside the sector between c and $-c$, with monotonous stretching the void ratio is increasing and p' is decreasing (therefore these states cannot be approached from a stress-free state), $e < e_c$ holds and thus $r_e < 1$. These state limits come close to *peak states*, states of maximum $|\psi_\sigma|$ and $|\psi_{\dot{\epsilon}}|$ achieved in shear tests with constant

[1] Version with constant Poisson ratio ν is used, the elastic shear stiffness predicted by the model is therefore proportional to the mean stress $p' = (\sigma'_1 + 2\sigma'_2)/3$

$\psi_{\dot{\sigma}}$ (defined equivalently to ψ_σ and $\psi_{\dot{\epsilon}}$). *Axial splitting* with $\sigma'_2 = 0$ and $\dot{\epsilon}_1 = 0$ and *discing* with $\sigma'_1 = 0$ and $\dot{\epsilon}_2 = 0$ (labelled d and $-d$) are not attainable limit bounds. They are related with a lower bound void ratio e_d, i.e. with $r_e = 0$.

Comparison of constitutive models

In the following, we show how the proposed graphical representation can be used for comparison of response capabilities of different constitutive models. Three models of different mathematical and same physical bases have been chosen – the already mentioned Modified Cam clay model (Roscoe and Burland 1968), a hypoplastic model for granular materials (von Wolffersdorff 1996) and a hypoplastic model for clays (Mašín 2005, Mašín 2007). The models have all been calibrated to represent the behaviour of one specific soil (Beaucaire Marl, see Mašín et al. 2006); the calibration and parameter values are not detailed here, as they are not important for qualitative comparison of the model responses.

Response envelopes by the two hypoplastic models are shown in Fig. 5. They are plotted for the same initial states as used in Fig. 3, thus enabling a direct comparison with the response by the Modified Cam clay model. Figure 5 demonstrates that the response envelopes predicted by the hypoplastic models are elliptic. Unlike in elasto-plasticity, however, the ellipses are not centred about the reference state, so different tangential stiffnesses are predicted for different stretching directions (thus these models are *incrementally nonlinear*). It may be noticed that the translation with respect to the reference state decreases with increasing overconsolidation from *i*, through *oc1* to *oc2*, representing the influence of overconsolidation ratio (or relative density). The influence of the mean stress, similar to the Modified Cam clay model in Fig. 3, is revealed by the size of the envelopes. It may also be seen that for critical states ($\pm c$) the response envelopes are shifted in such a way that they touch the reference state in the point corresponding to $\psi_{\dot{\epsilon}}(\pm c)$ (see Fig. 2 for labels). The models therefore predict zero stress rates for constant volume stretching, as required for critical state conditions.

Using a representation as in Fig. 4, state limits predicted by the three constitutive models are shown in Fig. 6. (void ratio limits as by Fig. 4a are omitted). As the Modified Cam clay and Mašín's models do not specify a lower bound e_d for the void ratio, r_e in Eq. (5) was substituted by $r_e = e/e_c$. Note that in the case of these two models the graph of Fig. 4b is due to the logarithmic compression law not unique for different p'. These models are formulated in such a way that the state limits can be represented uniquely in an alternative graph (not presented here) with r_e substituted by p_e/p', were p_e is Hvorslev's (1937) equivalent pressure. It may be noticed that the curve by the Modified Cam clay model is not bound by directions $-d$ and d of ψ_σ from Fig. 1a as is the curve by the Mašín's model. This is because the elliptic yield surface of the Modified Cam clay model does not exclude tensile stresses (see Fig. 3). Also, this elliptic yield surface implies an overprediction of the critical state friction angle in extension, which is manifested by different ψ_σ for points $-c$ in Fig. 6b for the Modified Cam clay and other two models, which assume the same φ_c for compression and extension. The curves in Fig. 6a are similar for the three models. This indicates that the strain rate direction for state limits, implied by the flow rule and elasticity in the case of the elasto-plastic Modified Cam clay model, is predicted similarly by the hypoplastic models. Fig. 6 shows also that the $\psi_{\dot{\epsilon}}$ directions d and $-d$ of Fig. 1b do not correspond exactly to directions ψ_σ as defined in Fig. 1a and to $r_e = 0$. Thus the unattainable limits $\pm d$ are not incorporated precisely into the three studied constitutive models.

To demonstrate asymptotic properties of the three constitutive models considered, approaches to state limits predicted by them are plotted in Fig. 7 in planes of stress components (a, c, e) and void ratio versus mean pressure (b, d, f) for three strain paths directions. Direction A is contractant and corresponds to K_0 conditions with $\psi_{\dot{\epsilon}}(A) \simeq 54.7°$, direction

B is isochoric and corresponds to direction c with $\psi_{\dot{\epsilon}}(B) = 90°$, direction C is dilatant with $\psi_{\dot{\epsilon}}(C) = -110°$. Initial states do not correspond to state limits. The state limits according to Fig. 6 are included as thin dotted lines in Fig. 7. They are *attractors*, i.e. they are reached by proportional stretching (constant $\psi_{\dot{\epsilon}}$) independently of the initial state. Fig. 7 shows how paths predicted by the models tend to these asymptotes.

Concluding remarks

In this Note, we propose graphical representations of basic properties of constitutive rate equations, namely tangential stiffness and state limits. The proposed approach can be used to represent different constitutive models without need for understanding details of their algebraic representations, and thus simplifies judgement of their response capabilities. Using the proposed representation we have demonstrated that the Modified Cam clay model and the selected hypoplastic models, though being fundamentally different algebraically, have the same physical grounds.

Acknowledgement

The second author highly appreciates financial support by the research grants GAAV IAA200710605 and MSM 0021620855.

References

Gudehus, G. (1979). A comparison of some constitutive laws for soils under radially symmetric loading and unloading. In *Proc. 3rd Int. Conf. on Numerical Methods in Geomechanics*, pp. 1309–1323. Aachen.

Gudehus, G. (2008). *Physical Soil Mechanics*. Springer, Berlin (in print).

Gudehus, G., M. Goldscheider, and H. Winter (1977). Mechanical properties of sand and clay and numerical intergration methods: some sources of errors and bounds of accuracy. In G. Gudehus (Ed.), *Finite Elements in Geomechanics*, pp. 121–150. Wiley.

Hvorslev, M. J. (1937). *Über die Festigkeitseigenschaften gestörter bindiger Böden*. Ph. D. thesis, Danmarks naturvidenskabelige samfund, København.

Mašín, D. (2005). A hypoplastic constitutive model for clays. *International Journal for Numerical and Analytical Methods in Geomechanics 29*(4), 311–336.

Mašín, D. (2007). A hypoplastic constitutive model for clays with meta-stable structure. *Canadian Geotechnical Journal 44*(3), 363–375.

Mašín, D., C. Tamagnini, G. Viggiani, and D. Costanzo (2006). Directional response of a reconstituted fine grained soil. Part II: performance of different constitutive models. *International Journal for Numerical and Analytical Methods in Geomechanics 30*(13), 1303–1336.

Roscoe, K. H. and J. B. Burland (1968). On the generalised stress-strain behaviour of wet clay. In J. Heyman and F. A. Leckie (Eds.), *Engineering Plasticity*, pp. 535–609. Cambridge: Cambridge Univesrity Press.

von Wolffersdorff, P. A. (1996). A hypoplastic relation for granular materials with a predefined limit state surface. *Mechanics of Cohesive-Frictional Materials 1*, 251–271.

List of Figures

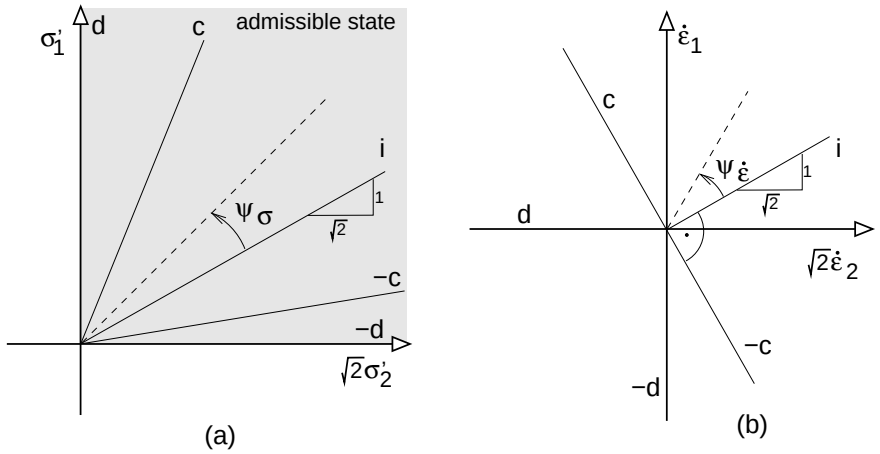

Figure 1: Definition of angles $\psi_{\dot{\epsilon}}$ and ψ_σ and special directions i, c, $-c$, d and $-d$.

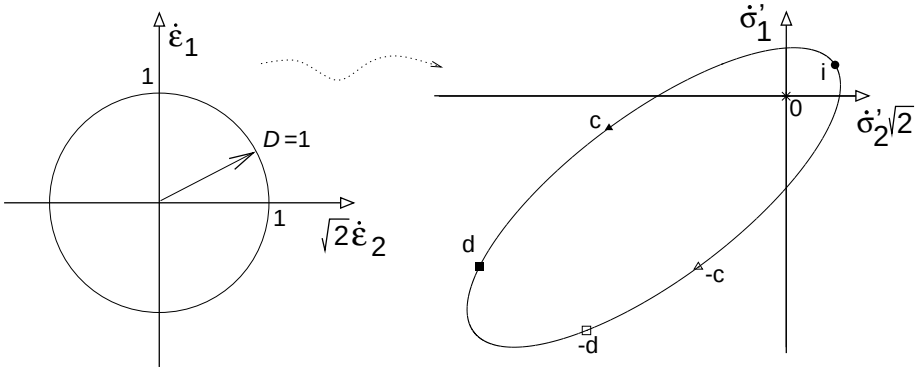

Figure 2: Response envelope of stress rates due to unit strain rates. Labels i, c, $-c$, d and $-d$ correspond to directions of $\psi_{\dot{\epsilon}}$ as defined in Fig. 1b.

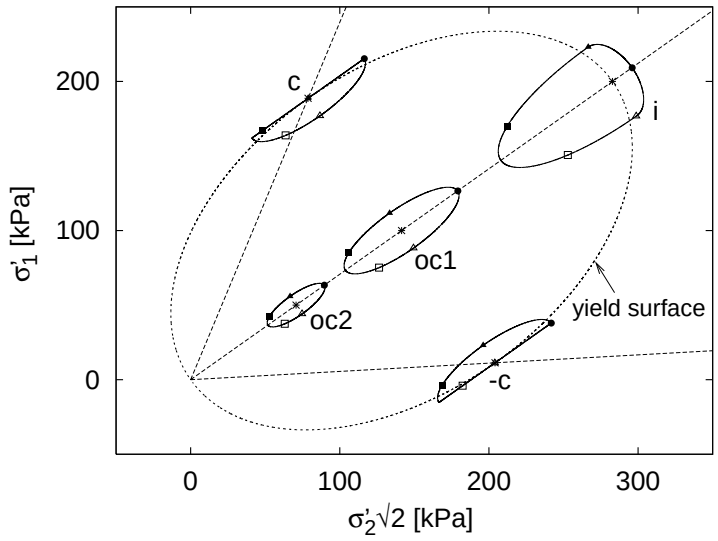

Figure 3: Response envelopes by the Modified Cam clay model for different initial states

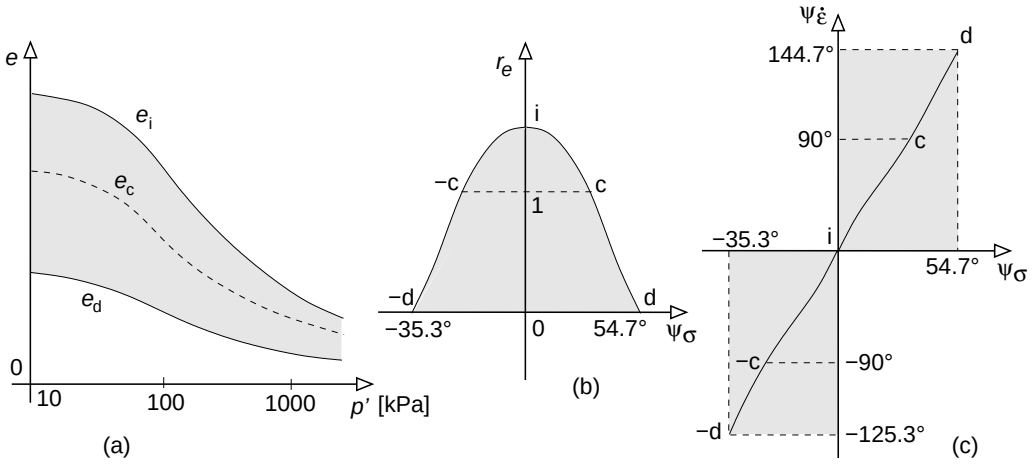

Figure 4: Graphical representation of state limits. Admissible states lie in grey zones.

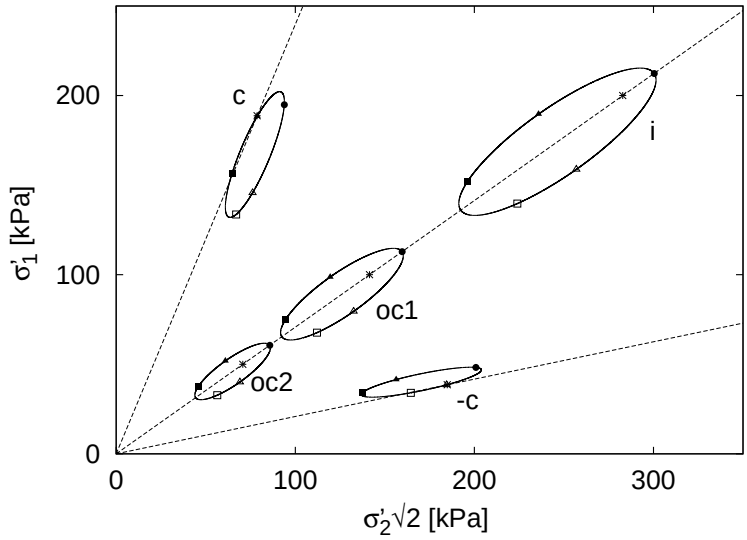

(a)

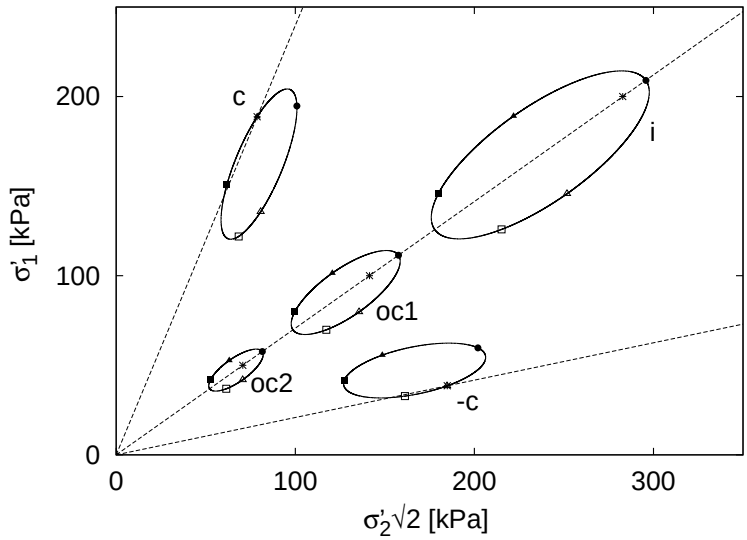

(b)

Figure 5: Response envelopes for von Wolffersdorff's (a) and Mašín's (b) hypoplastic models. Initial states the same as in Fig. 3.

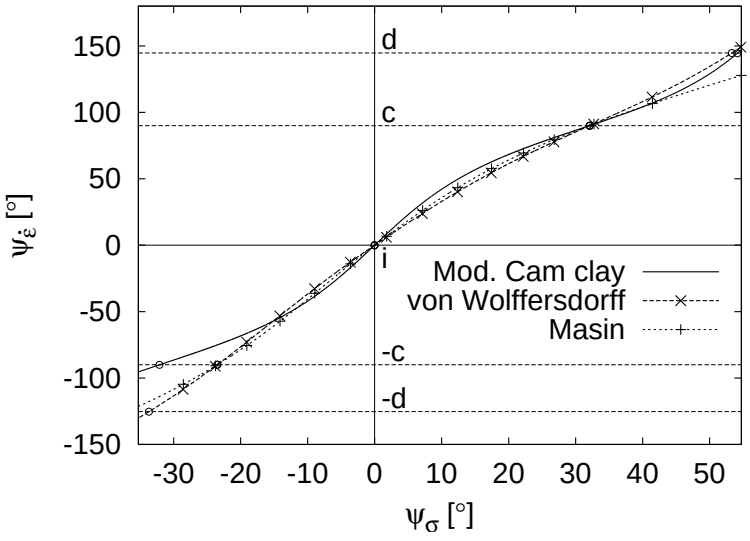

(a)

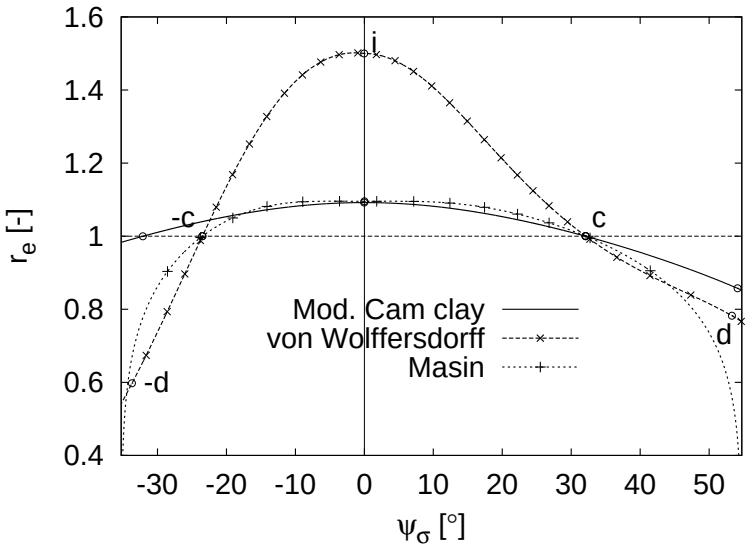

(b)

Figure 6: State limits as predicted by selected constitutive models, r_e in (b) for the Cam clay and Mašín's models plotted for $p' = 100$ kPa. Labels i, c, $-c$, d and $-d$ correspond to directions of $\psi_{\dot{\epsilon}}$ as defined in Fig. 1b

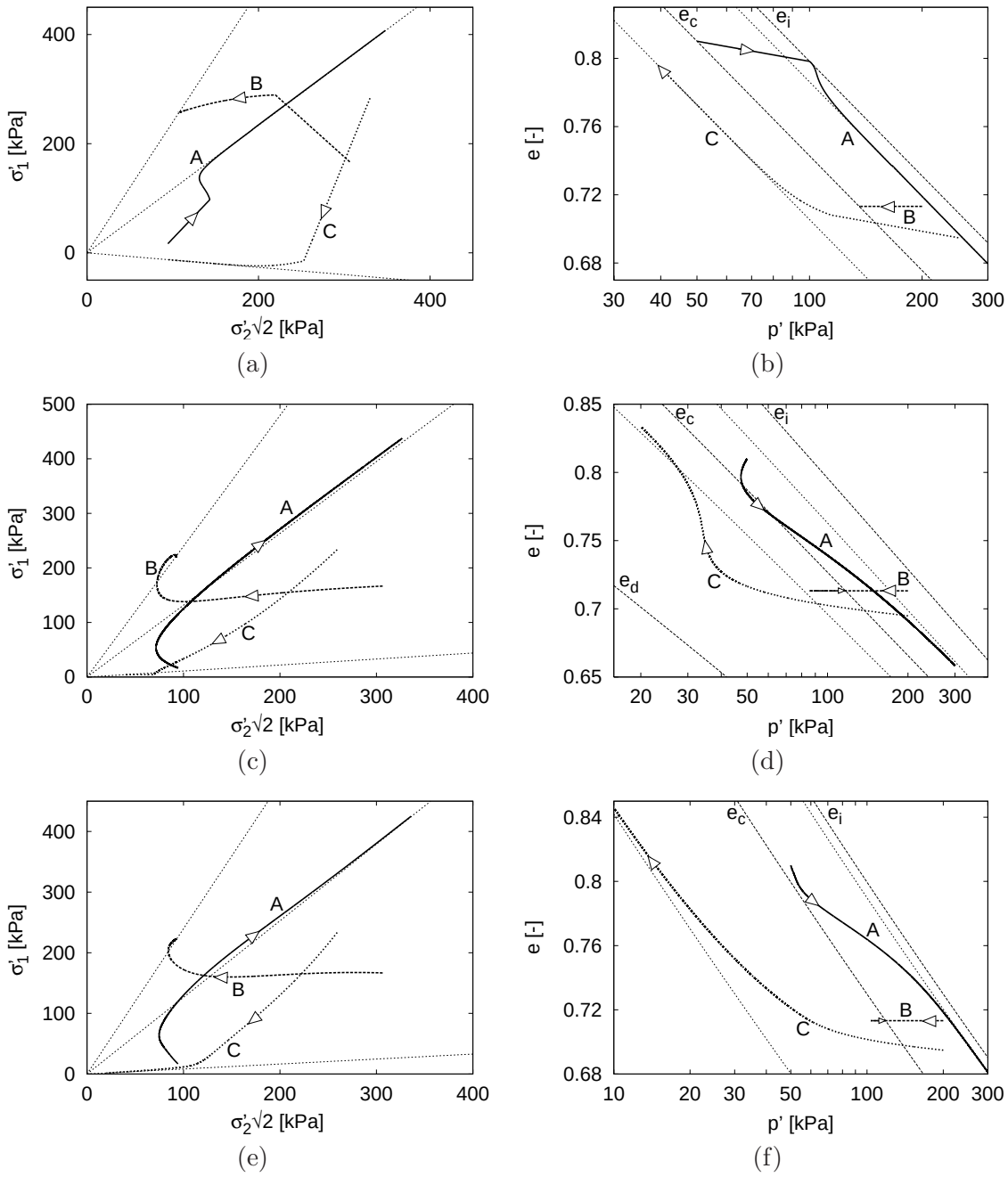

Figure 7: Asymptotic properties of the Modified Cam clay model (a, b), von Wolffersdorff's model (c, d) and Mašín's model (e, f). State limits corresponding to stretching directions A, B and C included as thin dotted lines, void ratio limits e_i, e_c (and e_d) by thin dotted lines with labels.